Pure appl. geophys. 164 (2007) 1547–1576
0033–4553/07/091547–30
DOI 10.1007/s00024-007-0227-2

Pure and Applied Geophysics

Sensitivity of Mesoscale Surface Dynamics to Surface Soil and Vegetation Contrasts over the Carolina Sandhills

RYAN BOYLES, SETHU RAMAN, and AARON SIMS

Abstract—A region of contrasting soils exists over the Carolinas region of the southeastern United States. Previous research has shown an increase in mesoscale summertime precipitation over this region. Numerical simulations are analyzed to investigate the relationships between mesoscale surface dynamics and the transition from clay to sandy soils over this region. Numerical modeling experiments using four different soil and vegetation patterns suggest that the presence of the clay-to-sand transition zone produces a surface heat flux gradient and enhanced convergence. The soil contrasts appear to dominate over vegetation contrasts in affecting local surface heating and convergence in the model atmosphere.

Key words: Land surface variation, North Carolina, soils.

1. Introduction

In the southeastern United States, there exists a region of sharp change from dense clay soils to coarse sandy soils. This region is known as the Carolina Sandhills for its rolling sandy hills stretching from eastern North Carolina (NC) through South Carolina (SC) and Georgia (GA). The Sandhills region of the Carolinas lies along a zone generally parallel to the coastline and inland approximately 160 kilometers (100 miles) from the Atlantic Ocean. The transition from clay soils in the Piedmont region of the Carolinas to the Sandhills is believed to play a role in local precipitation dynamics.

The influence of soil type and land use variation on lower atmospheric energy exchange has been well documented (DEARDORFF, 1978; ANTHES, 1984; OOKOUCHI *et al.*, 1984; MAHFOUF *et al.*, 1987; SEGAL *et al.*, 1988; HONG *et al.*, 1995). KOCH and RAY (1997) documented a region of low pressure that forms during summers along the boundary of the Piedmont and Coastal Plain of North Carolina. This "Piedmont Trough" was found to be present 40% of the time during summer when convection occurred. KOCH and RAY (1997) found the "Piedmont Trough" to produce convection in the absence of other forcing boundaries, such as cold fronts or

State Climate Office of North Carolina, Department of Marine, Earth, and Atmospheric Sciences, North Carolina State University, Raleigh, NC 27695-7236, U.S.A.

sea-breeze fronts. KOCH and RAY (1997) determined that the "Piedmont Trough" enhanced convection in the presence of sea-breeze fronts, and that this region was second only to the sea-breeze as a source for summertime convective forcing.

More recently, RAMAN *et al.* (2005) used a summer climatology of National Weather Service Cooperative Observer gages and numerical model simulations to conclude that the contrasting soils and vegetation produce "significant horizontal gradients in the latent and sensible heat flux patterns in the Sandhills" and that these "contribute to the development of mesoscale circulations observed in this region".

The mesoscale dynamics associated with the Sandhills are further explored here using results from a numerical weather modeling study to identify the sensitivity of boundary-layer processes to the soil and vegetation variations of the Sandhills during a summertime event with weak synoptic flow.

2. Numerical Modeling Experiments

Observations of MPE on climatological scales suggest an increase in precipitation over the Sandhills region of the Carolinas (RAMAN *et al.*, 2005). A possible reason for this observed increase is enhanced convection due to the formation of a locally-forced thermal gradient and resulting vertical circulation, similar to a sea-breeze. A conceptual schematic of this circulation is provided in Figure 1. However, it is not known if the boundary layer and local circulations are more sensitive to the soil transition or the vegetation transition in this region. A series of numerical simulations are performed to investigate the sensitivity of the lower troposphere to soil and vegetation contrasts in the Sandhills. Using a numerical weather model, soil

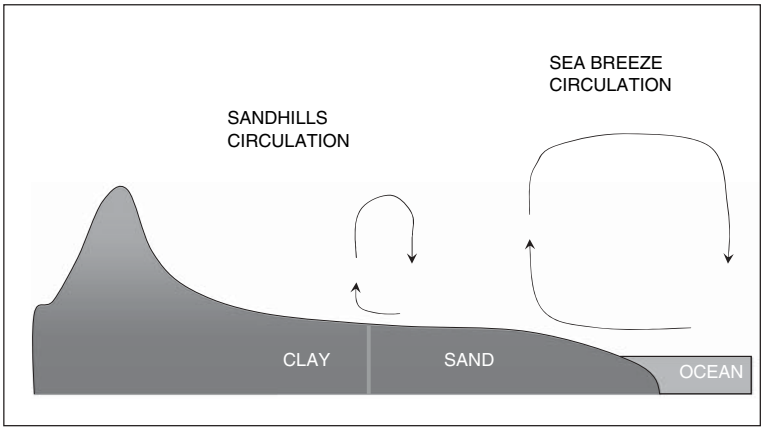

Figure 1
Diagram of the sea breeze and proposed Sandhills thermal circulations. Just as differential heating between land and water produces the classic sea breeze circulation, differential heating over different soil types may produce a circulation over the Sandhills region of the Carolinas.

and vegetation patterns are changed to identify the sensitivity of the boundary layer to the variation in land use and soil patterns that are typical of the Sandhills region. Specifically, the soil type and vegetation in the model are modified to remove the clay-to-sand transition zone and the vegetation contrasts and compare the results with a control simulation that includes standard soil and vegetation patterns.

2.1. Model Description

MM5 version 3.7 was used to simulate the atmosphere and surface dynamics for the period July 9–13, 2004. GRELL *et al.* (1995) provides details on the MM5 numerical weather modeling system. MM5 uses a sigma coordinate system that follows the terrain and a finite fixed resolution grid to solve the general atmospheric equations of motion, thermodynamics, and state.

For this study, a one-way single nest is used. The model domain is shown in Figure 2, with an outer domain grid spacing of 12 km and inner domain grid spacing of 4 km. 42 vertical levels were used, with 25 below 700 mb. Terrain, soil, and land-use data were obtained from the National Center for Atmospheric Research (NCAR)

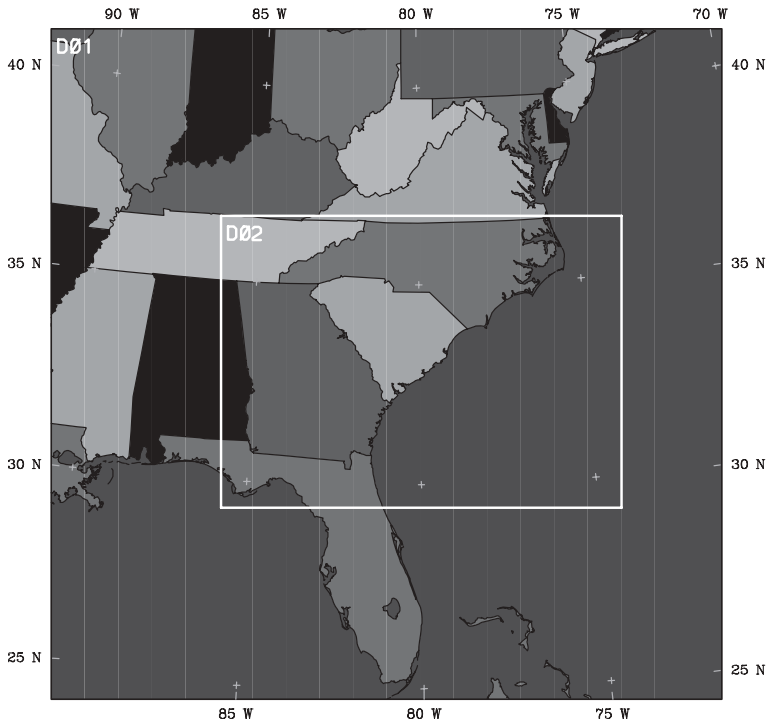

Figure 2
Outer and inner domains for MM5 simulations. The outer domain uses a 12-km grid spacing while the inner domain uses a 4-km grid spacing.

and use the 24-class vegetation/land use reference and 19-class dominant soils reference as developed by the US Geological Survey (USGS). The model vegetation pattern is shown in Figure 3 and dominant soil pattern is shown in Figure 4. The model characteristics associated with each land use/vegetation class are listed in Table 2, while model characteristics for each soil class are given in Table 1. The model physics options used for these simulations are given in Table 3. In all simulations, Reisner's mixed phase precipitation physics scheme, the Medium-Range Forecast planetary boundary layer (MRF PBL) scheme, the Rapid Radiative Transfer Model (RRTM) radiation scheme, and the NOAH land surface model were used. In the outer domain (155×155, 12-km grid spacing) the Kain-Fritsch 2 cumulus parameterization was used while the inner domain (202×277, 4-km resolution) used explicit cloud physics to resolve convection. Initial and lateral boundary conditions are derived from 3-hourly analyzed fields from the Eta Data Assimilation System (EDAS). Surface observations are assimilated into the model at three-hour time steps using available data from the in-house database at the State Climate Office of North Carolina. These observations, which include soil temperature and soil moisture data from the North Carolina Environment and Climate Observations Network (NC ECONet), are "nudged" into the model using the LITTLE_R module in MM5. Data assimilation nudges the model solutions toward observations, but does not shock the

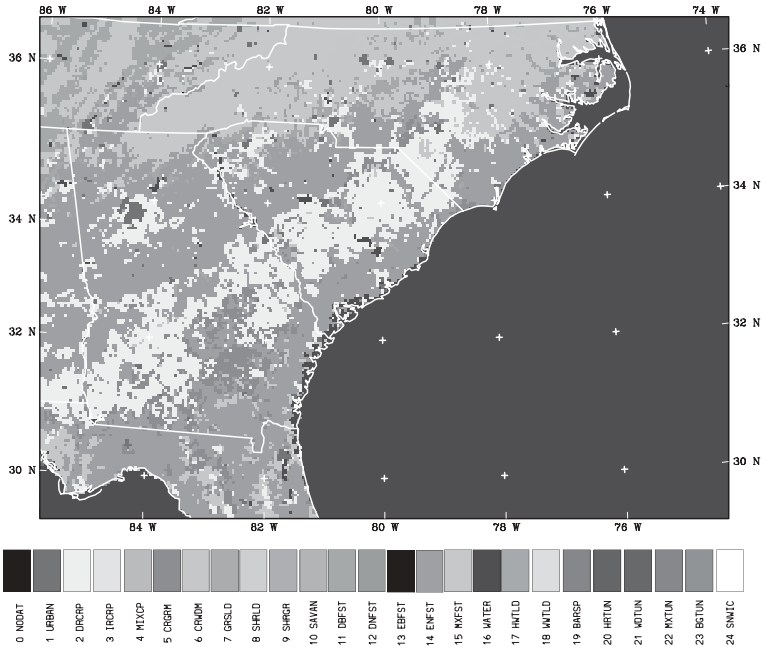

Figure 3
MM5 vegetation/land use classifications for the inner 4-km domain. Vegetation/land-use classes are described in Table 2.

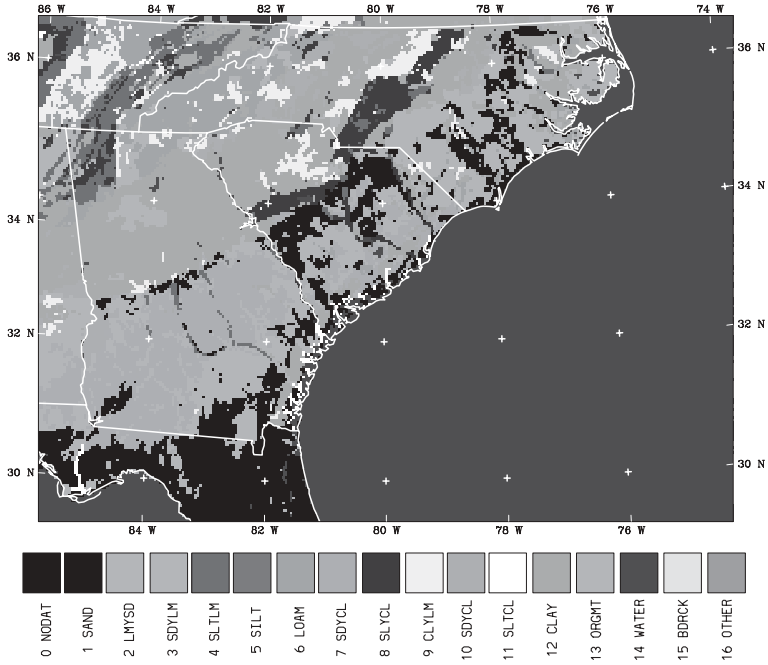

Figure 4
MM5 dominant soil classification for the inner domain. The soil classification properties are described in Table 1.

model with forced data, and therefore limits any spurious effects. A 24-hour model spin-up period is used prior to the period of analysis.

2.2. Synoptic Conditions

The period July 10–13, 2004 is chosen for simulations because there was weak synoptic forcing typical of summertime in the Carolinas and convection was observed in the satellite and radar imagery over the Sandhills region. Winds aloft are generally from the west to northwest over the 4-day period. Satellite imagery indicates generally clear conditions during the morning and early afternoon hours of July 10–13, 2004 over the Sandhills region (not shown). Each afternoon, convection forms over the Sandhills region, and then dissipates overnight. Convection is observed over the Sandhills and/or coastal plain on each day, but only July 12 is used for discussion of the modeling experiments.

2.3. Experimental Design

To investigate the sensitivities of the model atmosphere to soil and vegetation patterns, a series of four simulations are performed using MM5. The experimental

Table 1

Physical attributes associated with soil classes

USGS Soil Class	Soil Label	Slope of the Retention Curve	Wilting Point ($m^3\ m^{-3}$)	Soil Thermal Diffusivity / Conductivity Coefficient	Volumetric Water Content at Saturation ($m^3\ m^{-3}$)	Reference Field Capacity ($m^3\ m^{-3}$)	Saturated Soil Suction (m)	Hydraulic Conductivity at Saturation ($m\ s^{-1}$)	Soil Diffusivity Coefficient	Soil quartz content (%)
1	Sand	2.79	0.010	0.472	0.339	0.236	0.069	1.07E-06	6.08E-07	0.92
2	Loamy Sand	4.26	0.028	1.044	0.421	0.383	0.036	1.41E-05	5.14E-06	0.82
3	Sandy Loam	4.74	0.047	0.569	0.434	0.383	0.141	5.23E-06	8.05E-06	0.60
4	Silt Loam	5.33	0.084	0.162	0.476	0.360	0.759	2.81E-06	2.39E-05	0.25
5	Silt Loam	5.33	0.084	0.162	0.476	0.383	0.759	2.81E-06	2.39E-05	0.10
6	Loamy Sand	5.25	0.066	0.327	0.439	0.329	0.355	3.38E-06	1.43E-05	0.40
7	Sandy Clay Loam	6.66	0.067	1.491	0.404	0.314	0.135	4.45E-06	9.90E-06	0.60
8	Silty Clay Loam	8.72	0.120	1.118	0.464	0.387	0.617	2.04E-06	2.37E-05	0.10
9	Clay Loam	8.17	0.103	1.297	0.465	0.382	0.263	2.45E-06	1.13E-05	0.35
10	Sandy Clay Loam	10.73	0.100	3.209	0.406	0.338	0.098	7.22E-06	1.87E-05	0.52
11	Silty Clay Loam	10.39	0.126	1.916	0.468	0.404	0.324	1.34E-06	9.64E-06	0.10
12	Clay	11.55	0.138	2.138	0.468	0.412	0.468	9.74E-07	1.12E-05	0.25
13	Organic Material	5.25	0.066	0.327	0.439	0.329	0.355	3.38E-06	1.43E-05	0.05
14	Water	0.00	0.000	0.000	1.000	0.000	0.000	0.00E+00	0.00E+00	0.60
15	Bedrock	2.79	0.006	1.111	0.200	0.170	0.069	1.41E-04	1.36E-04	0.07
16	Other (Land-Ice)	4.26	0.028	1.044	0.421	0.283	0.036	1.41E-05	5.14E-06	0.25
17	Playa	11.55	0.030	10.472	0.468	0.454	0.468	9.74E-07	1.12E-05	0.60
18	Lava	2.79	0.006	0.472	0.200	0.170	0.069	1.41E-04	1.36E-04	0.52
19	White Sand	2.79	0.010	0.472	0.339	0.236	0.069	1.07E-06	6.08E-07	0.92

Table 2

Physical attributes associated with vegetation/land use classes

USGS Vegetation Class	Vegetation / Land Use Label	Albedo (%)	Soil Moisture Availability Fraction	Surface Emissivity Fraction	Surface Roughness Length (cm)	Surface Thermal Inertia ($100\times$cal cm^{-2} K^{-1} s$^{-½}$)	Snow Cover Effect Fraction	Surface Heat Capacity (J m^{-3} K^{-1})
1	Urban and Built-Up Land	15	0.10	0.880	80	3	1.67	1.89E+06
2	Dryland Cropland and Pasture	17	0.30	0.985	15	4	2.71	2.50E+06
3	Irrigated Cropland and Pasture	18	0.50	0.985	10	4	2.2	2.50E+06
4	Mixed Dryland/Irrigated Cropland and Pasture	18	0.25	0.985	15	4	2.56	2.50E+06
5	Cropland/Grassland Mosaic	18	0.25	0.980	14	4	2.56	2.50E+06
6	Cropland/Woodland Mosaic	16	0.35	0.985	20	4	3.19	2.50E+06
7	Grassland	19	0.15	0.960	12	3	2.37	2.08E+06
8	Shrubland	22	0.10	0.930	5	3	1.56	2.08E+06
9	Mixed Shrubland/Grassland	20	0.15	0.950	6	3	2.14	2.08E+06
10	Savanna	20	0.15	0.920	15	3	2	2.50E+06
11	Deciduous Broadleaf Forest	16	0.30	0.930	50	4	2.63	2.50E+06
12	Deciduous Needleleaf Forest	14	0.30	0.940	50	4	2.86	2.50E+06
13	Evergreen Broadleaf Forest	12	0.50	0.950	50	5	1.67	2.92E+06
14	Evergreen Needleleaf Forest	12	0.30	0.950	50	4	3.33	2.92E+06
15	Mixed Forest	13	0.30	0.970	50	4	2.11	4.18E+06
16	Water Bodies	8	1.00	0.980	0.01	6	0	9.00E+25
17	Herbaceous Wetland	14	0.60	0.950	20	6	1.5	2.92E+06
18	Wooded Wetland	14	0.35	0.950	40	5	1.14	4.18E+06
19	Barren or Sparsely Vegetated	25	0.02	0.900	1	2	0.81	1.20E+06
20	Herbaceous Tundra	15	0.50	0.920	10	5	2.87	9.00E+25
21	Wooded Tundra	15	0.50	0.930	30	5	2.67	9.00E+25
22	Mixed Tundra	15	0.50	0.920	15	5	2.67	9.00E+25
23	Bare Ground Tundra	25	0.02	0.900	10	2	1.6	1.20E+06
24	Snow or Ice	55	0.95	0.950	5	5	0	9.00E+25

Table 3

Model physics schemes used in domains

Outer Domain (155 × 155–12 km resolution)	
Cumulus parameterization	Kain-Fritsch 2 (w/shallow convection) (KAIN and FRITSCH, 1993)
Precipitation microphysics	Reisner's mixed-phase (REISNER *et al.*, 1998)
Planetary boundary layer processes	MRF (HONG and PAN, 1996)
Surface layer processes	NOAH land-surface model (CHEN and DUDHIA, 2001)
Atmospheric radiation	RRTM long-wave (MLAWER *et al.*, 1997)
Inner Domain (202 × 277–4 km resolution)	
Cumulus parameterization	Explicit cloud physics (SCHULTZ, 1995)
Precipitation microphysics	Reisner's mixed-phase (REISNER *et al.*, 1998)
Planetary boundary layer processes	MRF (HONG and PAN, 1996)
Surface layer processes	NOAH land-surface model (CHEN and DUDHIA, 2001)
Atmospheric radiation	RRTM long-wave (MLAWER *et al.*, 1997)

design for the four sensitivity simulations, including the differences in model soil and vegetation/land use for each simulation, is given in Table 4. In the CONTROL simulation, the reference USGS vegetation and soil spatial patterns are used. In CASE1, the USGS reference vegetation classes are used and all soils in the inner and outer domains are assigned as sand. Sand is used since it is typical of eastern NC (Sandhills area and east). Therefore, CASE1 has a uniform soil pattern but maintains a variation in vegetation. In CASE2, vegetation over land is prescribed to be only mixed forest and soils to be all sand. A mixed forest vegetation class is used since it is typical of vegetation in central and western NC, and is appropriate to represent typical vegetation dynamics across the southeastern US. In CASE2, uniform soil (sand) and uniform vegetation (mixed forest) are used in both the inner and outer domain of the model. In CASE3, the USGS standard soils are used, but the vegetation surface is changed to mixed forest, creating uniform vegetation but variations in soil. Each of the four model simulations is analyzed to investigate differences in surface convergence, wind fields, and heat fluxes, and regional precipitation amounts. By adjusting only the soil and vegetation patterns

Table 4

Experimental design for simulations

SIMULATION	SOIL	VEGETATION/LANDUSE
Reference (CONTROL) Case	USGS Standard	USGS Standard
CASE1	Sand	USGS Standard
CASE2	Sand	Mixed Forest
CASE3	USGS Standard	Mixed Forest

in each simulation, the resulting changes in atmospheric dynamics can be isolated as contributions from soil variation, vegetation variation, or both.

3. Discussion of Model Results

3.1. Control Simulation and Validation

A control simulation of the atmosphere is performed using the standard USGS soil and vegetation layers. Over the five-day study period, July 12 is used for analysis and discussion. To evaluate the model performance on this day, atmospheric profiles and surface measurements from the control simulation are compared with observations.

Analysis of model profiles compared with radiosonde observations (not shown) for Charleston, SC (CHS) and Greensboro, NC (GSO) show the model overall does a good job of simulating the wind and thermodynamic at heights above 1000 meters in the morning (08LT), though the northerly (-V) component of the wind is too strong through the entire troposphere. The model overestimates potential temperature and underestimates the mixing ratio near the surface. More importantly, the model does not properly capture the boundary layer inversion seen in the observed soundings.

A time history of the u and v components of the wind for the CONTROL simulation compared with observations for the Jackson Springs ECONet station (JACK) on July 12 is shown in Figure 5. Jackson Springs is located at latitude 35.18782° and longitude −79.68437° - in the middle of the Sandhills region of NC. Model simulated winds on July 12 overall have a northerly component that is too strong, but generally captures the weak U component over this day. Model simulated temperature and dew point for the entire four day simulation are shown in Figure 6. The model slightly overestimates the air temperature during the day and largely overestimates the temperature during nocturnal hours.

The model simulated 24-hour accumulated precipitation for July 12, 2004 is shown in Figure 7. Figure 8 shows the Multi-sensor Precipitation Estimated (MPE) total precipitation for July 12 (see LIN and MITCHELL, 2005 for more on MPE). The model captures the location of the daily precipitation in southeastern Georgia, northeast SC, and western NC, but missed the precipitation seen in MPE over central parts of NC and SC, and in northern Georgia. The CONTROL simulation produces precipitation over eastern NC that is not seen in MPE. The model also tends to produce much higher amounts in locations where rainfall is simulated–values often exceed one inch (25.4 mm) over areas where precipitation is simulated. In contrast, MPE shows a much smaller geographic area with amounts in excess of one inch (25.4 mm). However, it is rare that a model accurately represents both timing, location, and the amount of rainfall (especially convective

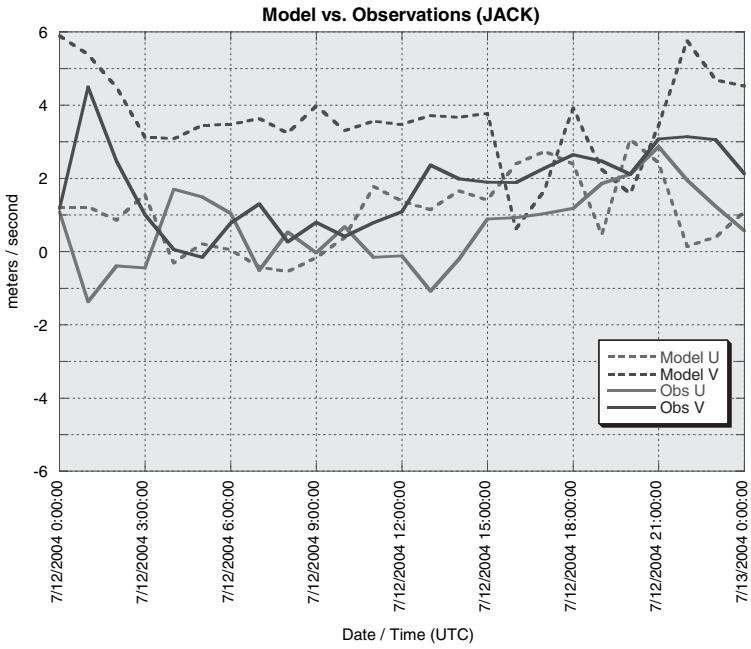

Figure 5
Time series of observed (solid) and model (dashed) wind components for the NC ECONet station at Jackson Spring, NC (JACK). The model 10 m winds generally simulate winds with a northerly component that is considerably stronger than actually observed.

precipitation). To better evaluate the performance of the model to simulate precipitation in general, spatially averaged rainfall amount from the model and observations are compared. The model does compare well with area-averaged precipitation amounts for July 10–12. The total areal average precipitation for the model over the region along and east of the Sandhills averages 0.3 inches (7.6 mm-17%) higher than observed. Although the control simulation does not accurately depict the timing and location of precipitation formation, the model predicted area-averaged precipitation amounts over the study area are not very different from observed values.

3.2. Sensitivity to Soil Type

To identify the sensitivity of the model atmosphere to soil variations, the control simulation is compared with a simulation of the atmosphere that maintains the vegetation variation but uses uniform sandy soils (CASE1). The two model simulations are compared at 14Z(10 LT) and 16Z (12LT) on July 12, 2004 using surface latent heat flux and surface sensible heat flux patterns, surface winds and convergence, and vertical cross sections.

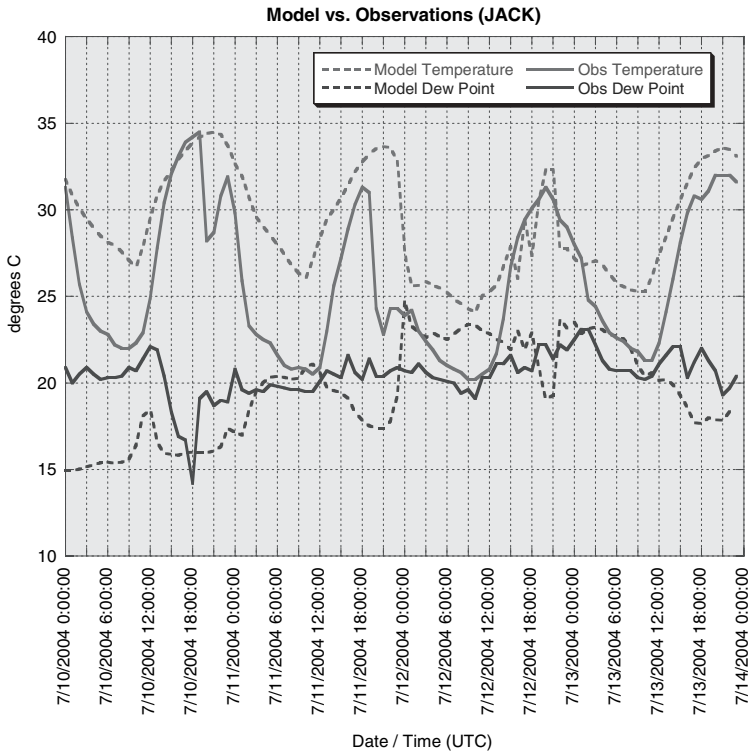

Figure 6
Time history of temperature and dew point recorded at a height of 2 meters for study period at the NC ECONet station at Jackson Springs, NC (JACK). Model temperatures are generally too warm during nocturnal hours, but capture the daytime temperatures fairly well.

In the CONTROL and CASE1 model simulations, surface latent heat fluxes (LHF) are generally uniform over land in both simulations during the nocturnal and early morning period with values between 25 and 50 W/m^2 (not shown). However, LHF variations do develop with sunrise and the heating of the day. Surface LHF at 14Z on July 12 is shown in Figure 9. A LHF difference is observed between the CONTROL and CASE1 simulations over areas west of the Sandhills. LHF values of 250 W/m^2 are observed in the CONTROL simulation over the region with clay soils, while in the sensitivity simulation with uniform sandy soils LHF values of 350 W/m^2 are observed in this same area. The differences over the Sandhills are more pronounced at 16Z (12LT) on July 12 (see Fig. 10). At this time in the CONTROL simulation, LHF of 150–250 W/m^2 is observed west of the Sandhills region, with LHF of 350–450 W/m^2 observed to the west and east of the clay-based soils. In the sensitivity simulation where all soils are sand, this gradient in LHF does not exist. Instead, LHF transitions from 450–500 W/m^2 in the west to 300–400 W/m^2 over

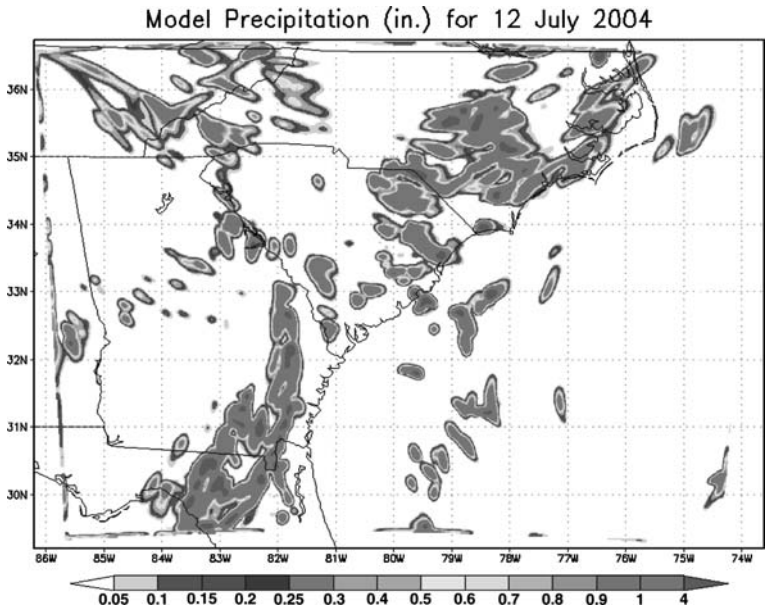

Figure 7
24-hour accumulation of model-simulated precipitation (in inches) using the CONTROL simulations.

eastern parts. Much lower values (< 200 W/m^2) are observed in both simulations over regions where the model simulates precipitation.

A contrasting pattern in sensible heat flux (SHF) is observed during the study period. During overnight hours, the sensible heat flux pattern is uniformly zero except for the higher SHF observed over the urban areas (less than 25 W/m^2 – figure not shown). As daytime heating begins, the sandy soil tends to heat slower than the clay-based soils. SHF patterns are shown for 14Z and 16Z on July 12, 2004 in Figures 11 and 12, respectively. In the CONTROL case, a SHF difference of 150 W/m^2 is observed between the clay soils and the Sandhills. In the Sand/Std. Vegetation simulation, a smaller difference of $\sim$50 W/m^2 is observed. At 16Z (12LT), the difference is more pronounced (see Fig. 12). Areas with clay soils in the CONTROL simulation have SHF values of $\sim$450 W/m^2, while in the sensitivity experiment with uniform sandy soils the SHF values over this region are generally less than 200 W/m^2.

Based on the latent and sensible heat flux patterns, a heat flux gradient associated with the clay-to-sand transition zone exists in the CONTROL simulation, but not simulated in the Sand/Std Vegetation sensitivity case. The heat flux gradient in the CONTROL simulation should be associated with surface convergence, while little or no convergence should be along the Sandhills in CASE1 since the heat flux gradient is weak.

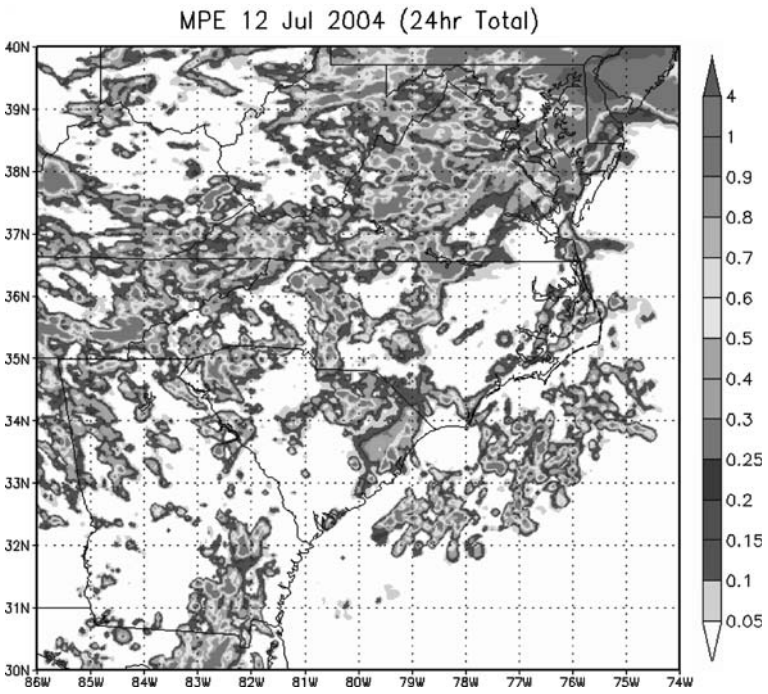

Figure 8
24-hour accumulated Multi-sensor Precipitation Estimates (MPE) (in inches).

Simulated wind vectors and convergence at 10 meters for the CONTROL and CASE1 simulations at 14Z and 16Z are shown in Figures 13 and 14, respectively. In both of these figures, strong convergence is observed over coastal areas and is associated with a sea breeze circulation. This circulation is not associated with dynamics along the Sandhills region. At 14Z (10 LT), wind vectors suggest convergence in NC and SC along the clay-to-sand transition. Wind vectors also appear to change in the sensitivity case, but the directional shift is less pronounced. However, at 16Z (12 LT), the differences between the two cases are obvious (see Fig. 14). At this time, a line of weak convergence and divergence is observed along the clay-to-sand transition zone in the CONTROL case with convergence values near 0.0004 s^{-1}. Convergence is generally on the west side of the transition, suggesting rising motion over the clay soils and sinking motion further east. This line of convergence is noticeably absent in the Sand/Std Vegetation sensitivity simulation.

Based on an analysis of the model surface heat fluxes, it is apparent that the model atmosphere is sensitive to soil variations and produces a surface heat flux gradient in the CONTROL simulation that is much weaker in the sensitively simulation. This gradient appears to be of sufficient strength to produce local convergence and a weak vertical circulation over the clay-to-sand transition zone in

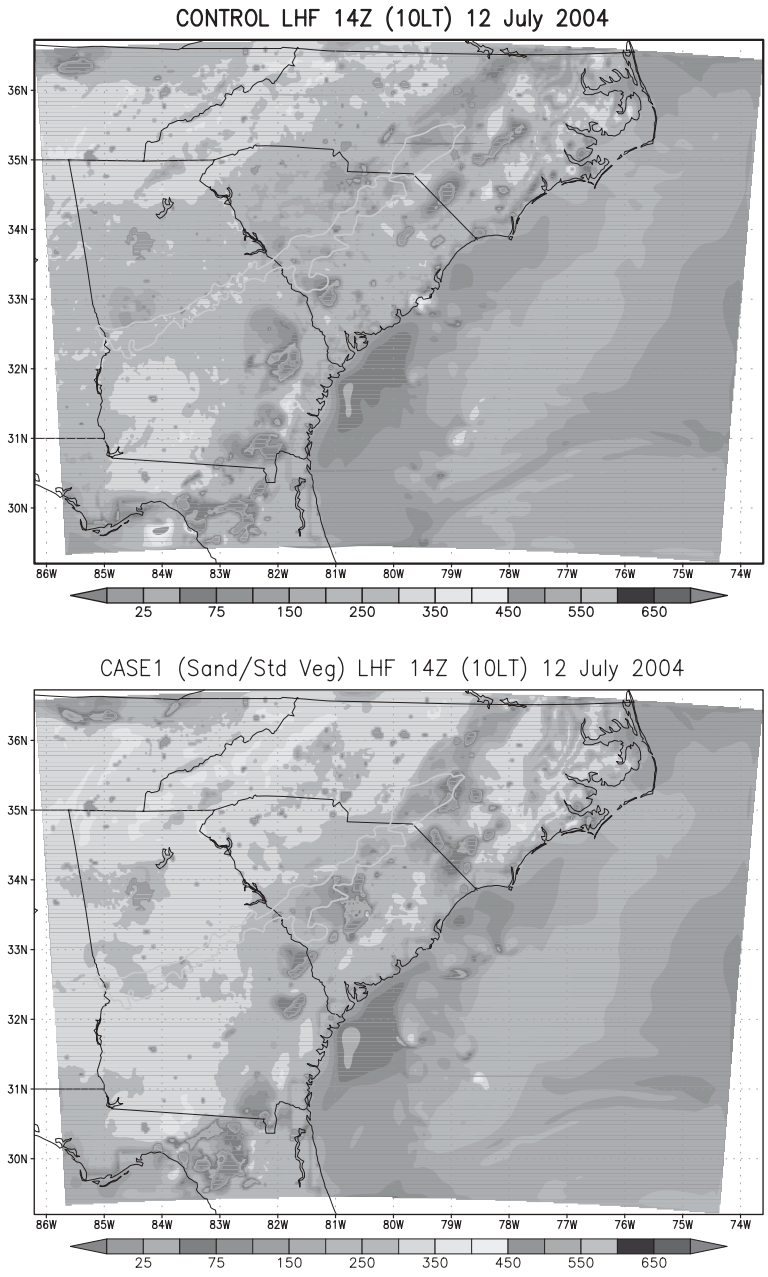

Figure 9
Surface latent heat flux (W/m^2) at 14Z (10LT) on July 12, 2004 for the CONTROL (top) and Sand/Std Vegetation (bottom) simulations. Differences in LHF are observed over the western parts of NC/SC/GA, where the clay soils exist in the CONTROL simulation but not in Case 2.

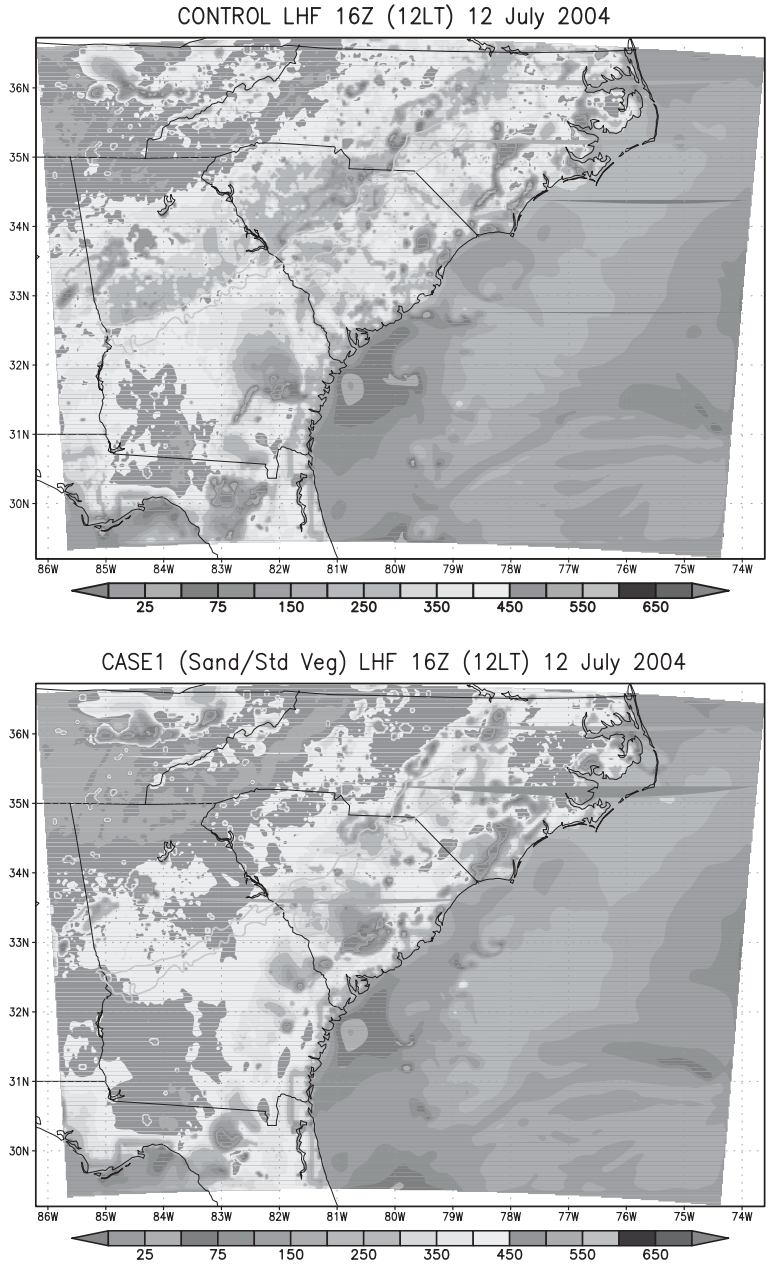

Figure 10
Surface latent heat flux (W/m^2) at 16Z (12LT) on July 12, 2004 for the CONTROL (top) and Sand/Std Vegetation (bottom) simulations. The heat-flux gradient that is observed in the CONTROL case is not observed in CASE1 west of the Sandhills.

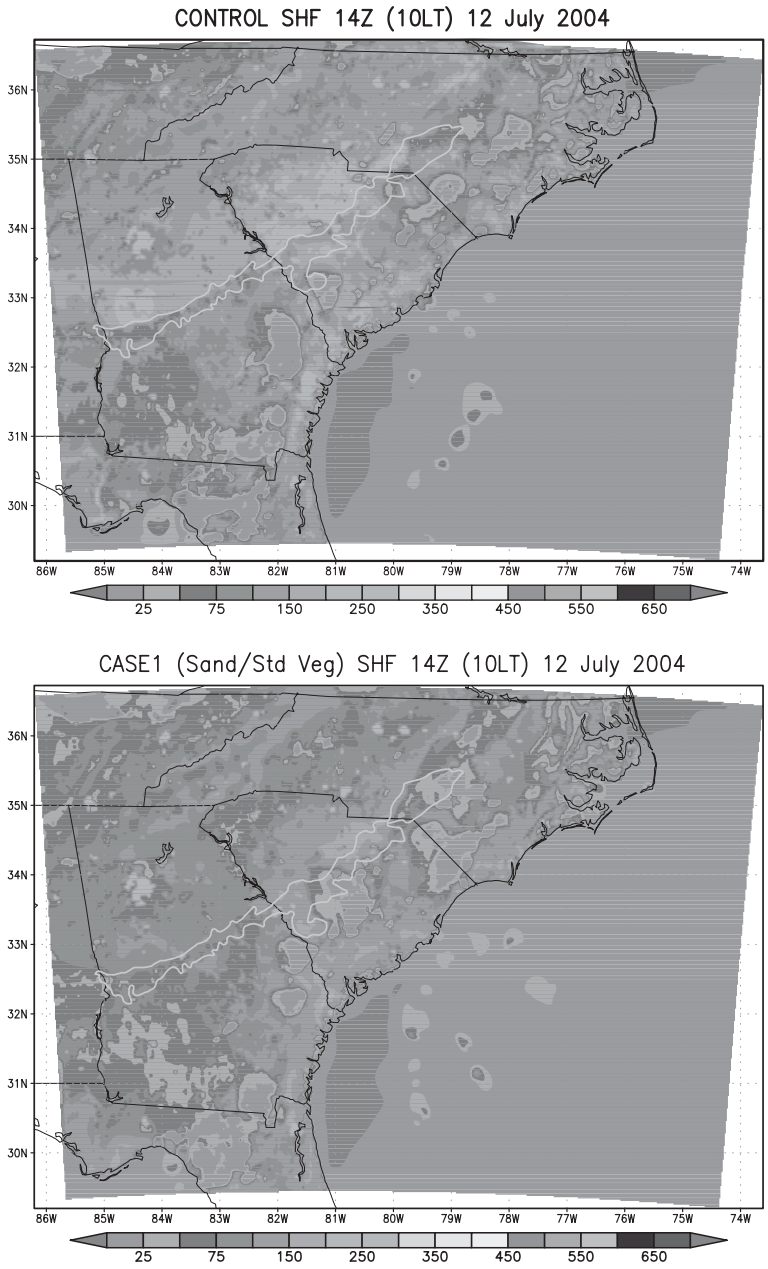

Figure 11
Surface sensible heat flux (W/m^2) at 14Z (10LT) on July 12, 2004 for the CONTROL (top) and Sand/Std Vegetation (bottom) simulations. Higher sensible heat fluxes are observed over the clay soils in the CONTROL simulation.

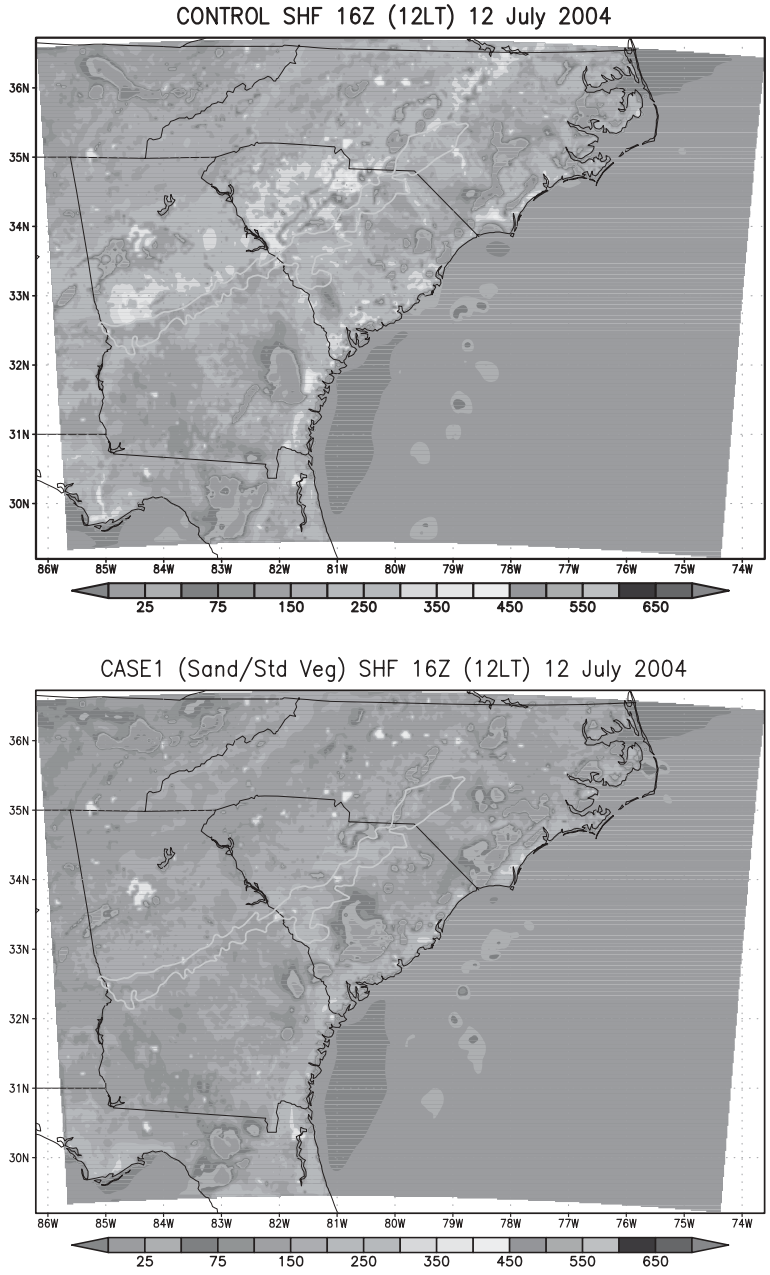

Figure 12
Surface sensible heat flux (W/m^2) at 16Z (12LT) on July 12, 2004 for the CONTROL (top) and Sand/Std Vegetation (bottom) simulations. The SHF gradient in the sensitivity simulation is not as large as in the CONTROL case.

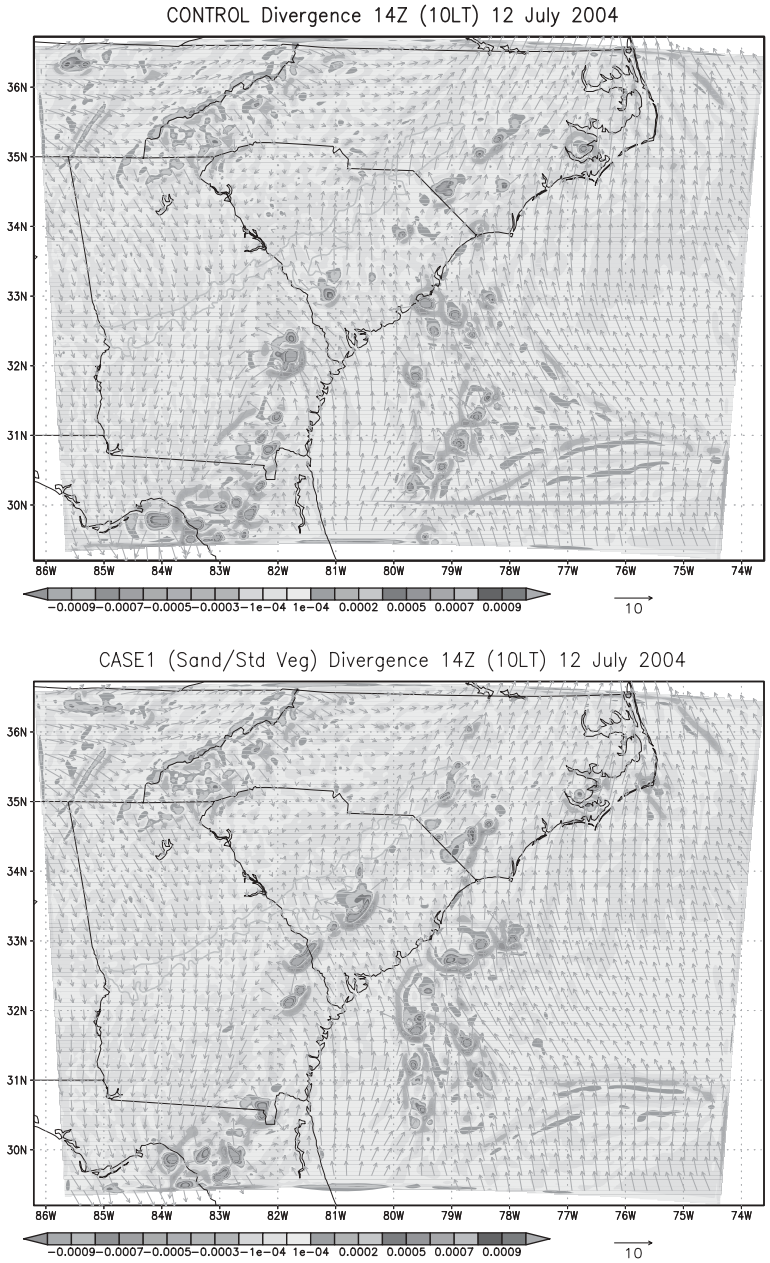

Figure 13
Surface winds and divergence for the CONTROL and CASE1 simulations at 14Z (10 LT) on July 12, 2004. Convergence is given as negative values (cool colors). Coastal convergence is associated with a sea breeze circulation.

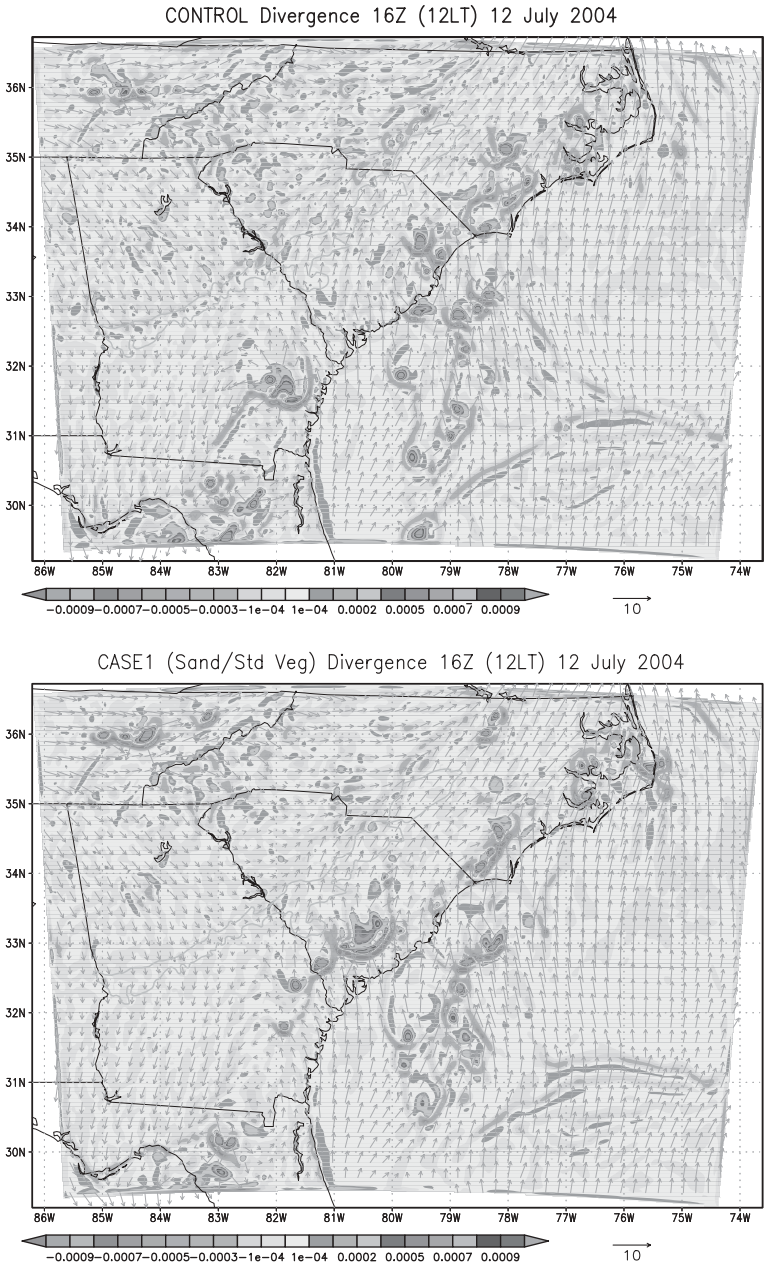

Figure 14
Surface winds and divergence for the CONTROL and CASE1 simulations at 16Z (12 LT) on July 12, 2004. A line of convergence through central NC/SC/GA is observed in the CONTROL case that is absent in the sensitivity case.

the CONTROL simulation. This feature is absent in the Sand/Std Vegetation sensitivity case.

3.3. Sensitivity to Vegetation/Land Use

While the analysis discussed in Section 3.2 offers strong evidence for the influence of the soils transition in the model simulation, contrasts in vegetation types over the region may also contribute to local heat flux gradients and local convergence. In order to identify the influence of vegetation contrasts compared with soil contrasts, two additional sensitivity simulations are performed. In CASE2, all soils are assigned as sand and the vegetation/land use classifications over land are prescribed as mixed forest (no contrast in soil or vegetation). In CASE3, the standard soils are used (same as in CONTROL) and the land use/vegetation is changed to mixed forest everywhere over land. CASE2 has uniform soils and uniform vegetation, while CASE 3 has uniform vegetation but varying soils. As in Section 4.2, latent heat flux, sensible heat flux, winds and convergence at the surface are analyzed at 14Z (10LT) and 16Z (12LT) on July 12, 2004. By comparing these two simulations with each other and the simulations discussed in Section 4.2, the dominant land surface influences may be evident.

As in the previous two sensitivity cases, latent heat flux (LHF) patterns in CASE2 and CASE3 during the overnight hours are generally uniform (25–50 W/m^2) across the domain (not shown). Differences between these two simulations are evident during the daytime hours. Figures 15 and 16 show the simulated surface latent heat fluxes at 14Z (10LT) and 16Z (12LT) on July 12, 2004 for CASE2 (Sand/Mixed Forest) and CASE3 (Std Soils/Mixed Forest), respectively. At this time, LHF of 50–100 W/m^2 are simulated over the clay-to-sand transition in SC and GA in CASE3, while no gradient is apparent in the Sand/Mixed Forest simulation (CASE2). At 16Z (12 LT), the LHF gradient along the Sandhills has increased to $\sim$ 200 W/m^2, while LHF values over central and eastern parts of the domain are generally uniform (except where rainfall is simulated). The LHF patterns in CASE3 (Std Soils / Mixed Forest) are very similar to the patterns observed in the CONTROL simulation (Figs. 9 and 10), and are not very different from the CONTROL as compared with the other two simulations.

The surface sensible heat fluxes (SHF) at 14Z and 16Z for CASE2 and CASE3 are shown in Figures 17 and 18, respectively. Similar to the latent heat flux pattern, a sensible heat flux pattern is seen along the Sandhills region in the simulation with contrasting soils (CASE3) at both 14Z and 16Z, ranging from 150–200 W/m^2. As with the latent heat flux, the sensible heat flux differences along the Sandhills in CASE3 are much closer in magnitude to the CONTROL simulation than the other sensitivity cases. Based on the surface heat flux patterns, it appears that the effect of the contrasting soils dominates over the vegetation contrasts to produce the heat flux gradient in the CONTROL simulation. Indeed, the SHF difference along the

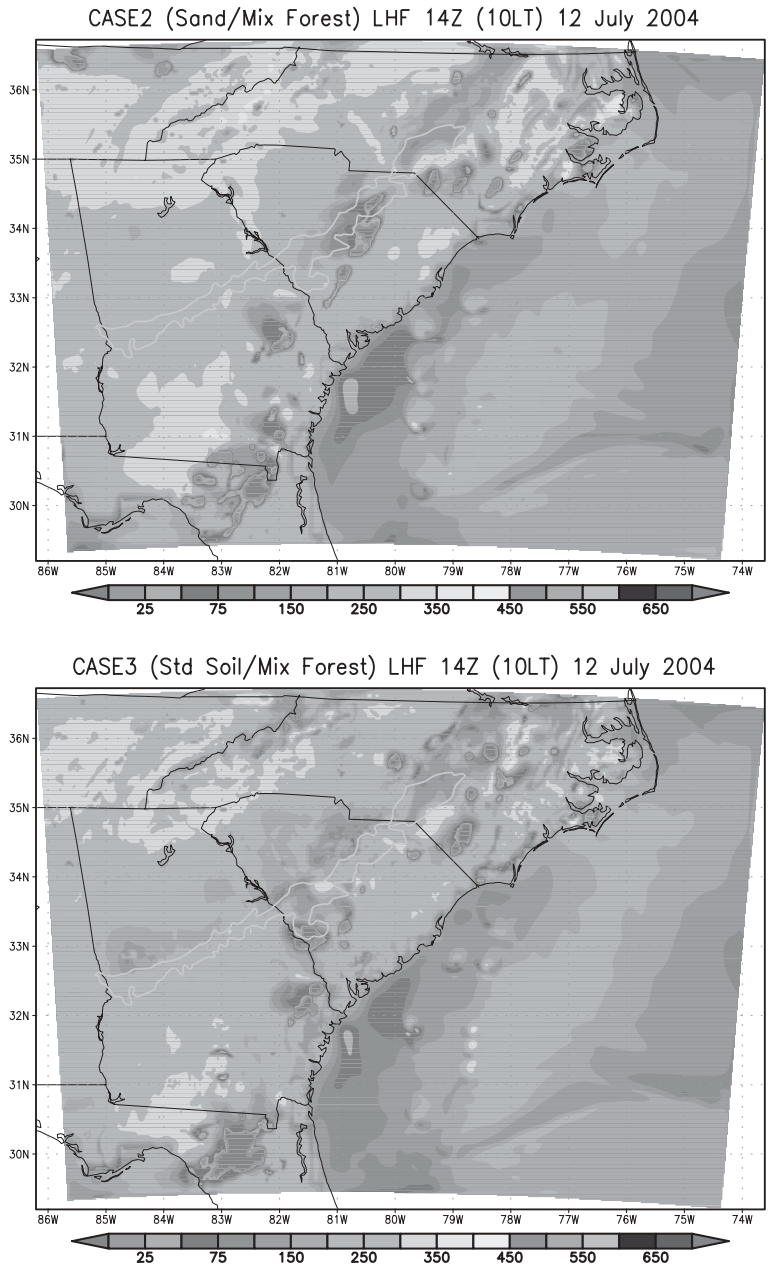

Figure 15

Surface latent heat flux (W/m^2) at 14Z (10LT) on July 12, 2004 for CASE2 (Sand/Mixed Forest) and CASE3 (Std Soils/Mixed Forest). LHF differences of 50–100 W/m^2 are observed over the clay-to-sand transition in SC and GA in CASE3, while no gradient is apparent in the Sand/Mixed Forest simulation. Values less than 100 W/m^2 are associated with recent rainfall over those areas.

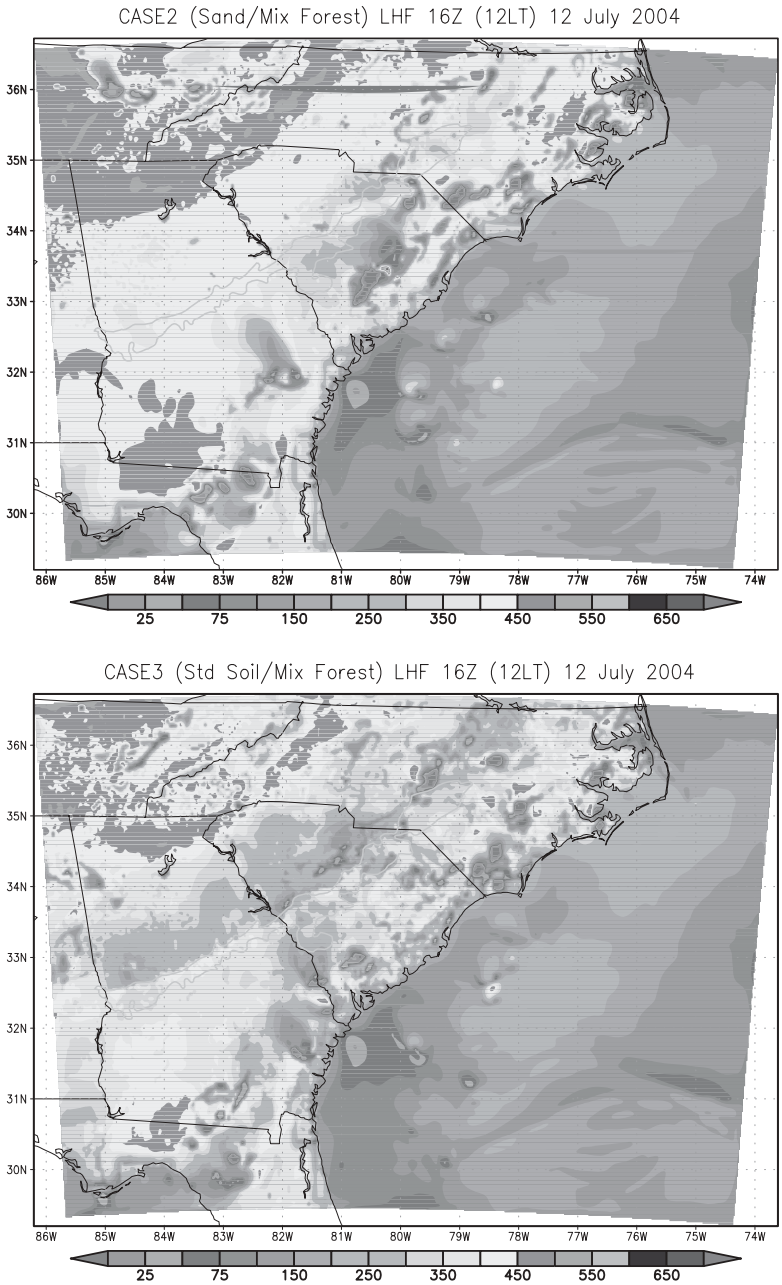

Figure 16

Surface latent heat flux (W/m^2) at 16Z (12LT) on July 12, 2004 for CASE2 (Sand/Mixed Forest) and CASE3 (Std Soils/Mixed Forest). LHF difference of 200 W/m^2 are observed over the clay-to-sand transition in SC and GA in CASE3. Values less than 100 W/m^2 are associated with recent rainfall over those areas.

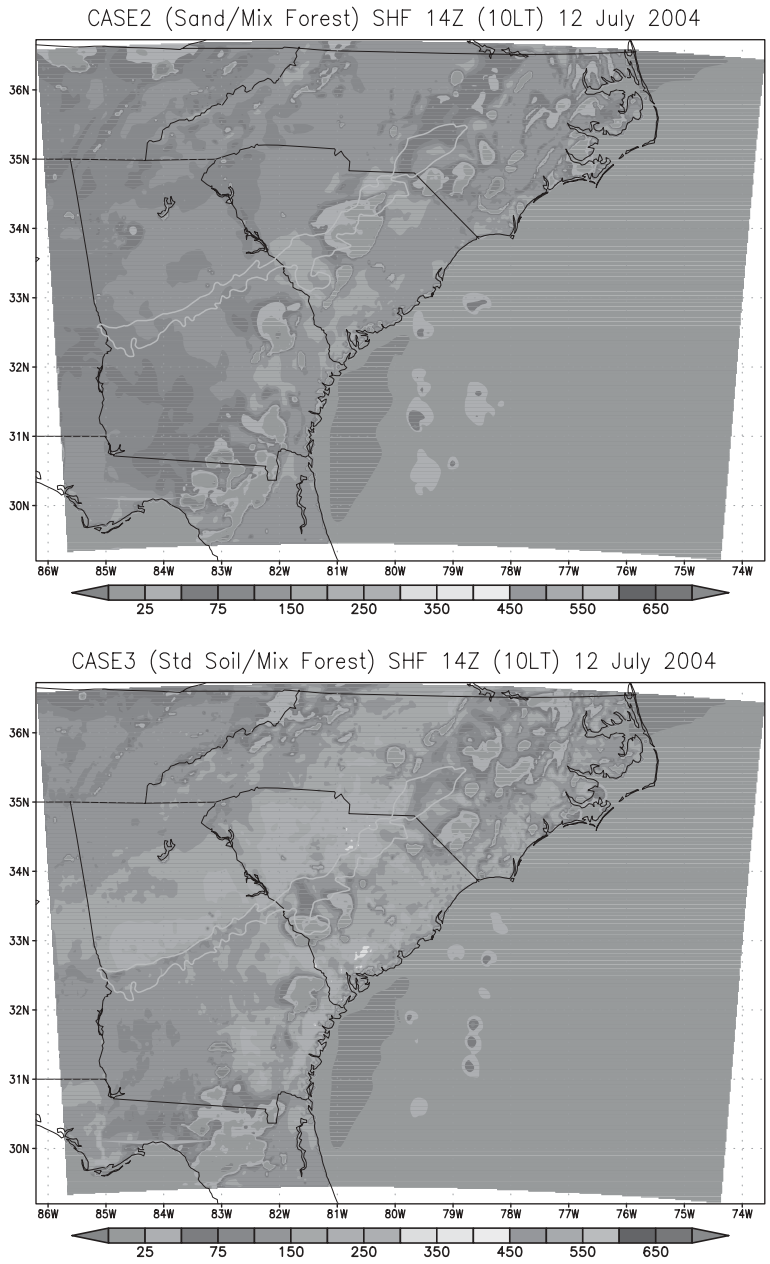

Figure 17
Surface sensible heat flux (W/m^2) at 14Z (10LT) on July 12, 2004 for CASE2 (Sand/Mixed Forest) and CASE3 (Std Soils/Mixed Forest). A gradient exists along the Sandhills in CASE3 that is not observed in CASE2.

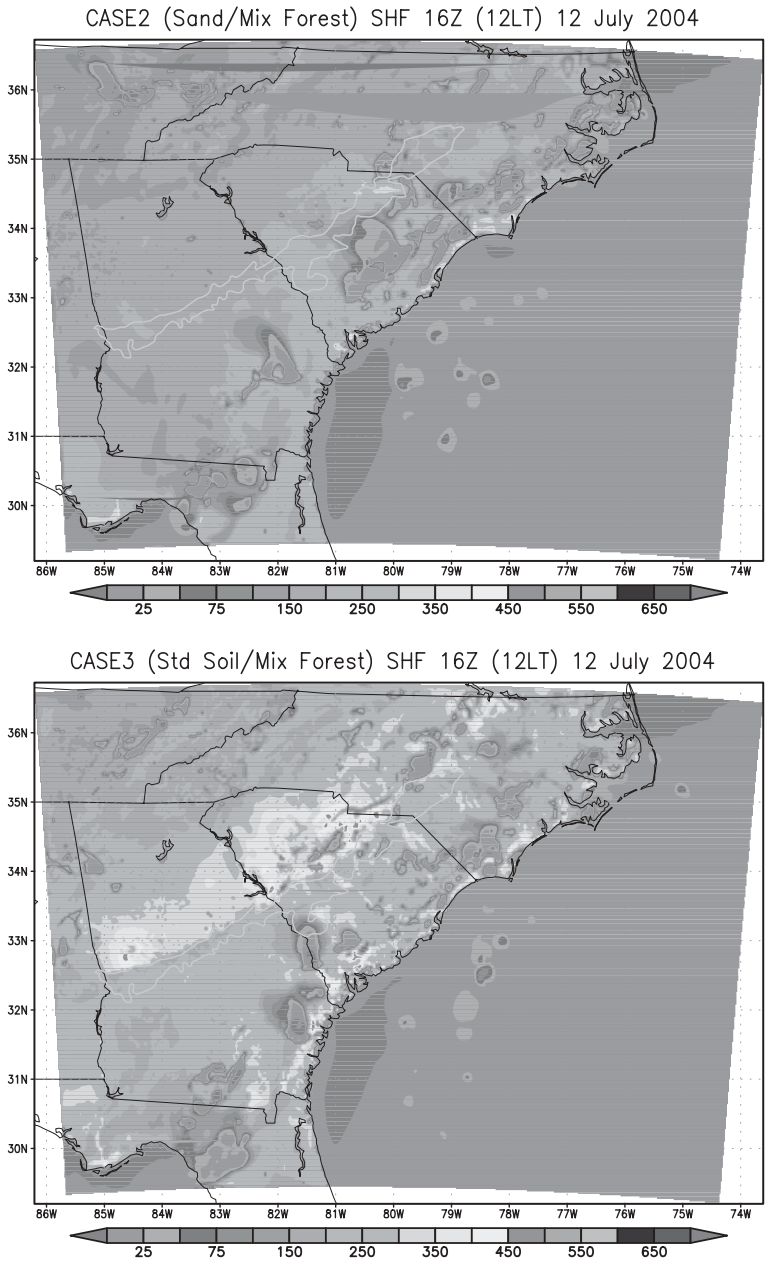

Figure 18
Surface sensible heat flux (W/m^2) at 16Z (12LT) on July 12, 2004 for CASE2 (Sand/Mixed Forest) and CASE3 (Std Soils/Mixed Forest). SHF gradients are similar to those observed in the CONTROL simulation.

Sandhills associated with the soil contrast is nearly 300% of the difference associated with the vegetation contrasts observed in CASE1 (Figs. 11 and 12).

Further analysis suggests that the heat flux gradients associated with the soils contrast along the Sandhills is sufficient to produce local convergence without the vegetation contrast. Figures 19 and 20 show the surface wind vectors and convergence for CASE2 and CASE3 on July 12, 2004 at 14Z and 16Z, respectively. Again, the patterns observed in CASE3 are similar to the CONTROL simulation. At 16Z (12LT) a local convergence zone along the Sandhills is observed just as in the CONTROL simulation. However, since CASE3 has a uniform vegetation surface, the convergence zone observed in CASE3 and the CONTROL simulation are likely forced by the soils contrast.

The differences in surface heat fluxes can largely be accounted for by differences in soil heat capacity. The surface energy budget for a layer has a relationship of the form:

$$R_N = H_S + H_L + H_G + \Delta H_S,$$

where R_N is net radiation, H_S is sensible heat flux, H_L is latent heat flux, H_G is ground heat flux, and ΔH_S is the change in the energy storage. The rate of change of energy storage of a soil layer is given as

$$\Delta H_S = \int \frac{\partial}{\partial t}(CT)\, dz,$$

where T is the absolute temperature of the soil layer and C is the heat capacity, which is a product of the mass density and specific heat of the soil. ARYA (2001) lists the heat capacity in $\mathrm{J\,m^{-3}\,K^{-1}} \times 10^6$ for dry (saturated) sand as 1.28 (2.96) and clay as 1.42 (3.10). The heat capacity for clay is approximately $0.14\,\mathrm{J\,m^{-3}\,K^{-1}} \times 10^6$ higher at both dry and saturated states. Thus, the rate of heating for a clay soil layer is between 5% and 11% higher than a sandy soil layer (depending on moisture content).

As described by CHEN and DUDHIA (2001), the model ground heat flux is based on a similar diffusion equation for soil temperature (T):

$$C(\Theta)\frac{\partial T}{\partial t} = \frac{\partial}{\partial z}\left(K_t(\Theta)\frac{\partial T}{\partial z}\right),$$

where C is the volumetric heat capacity and K_t is the thermal conductivity—both described as a function of Θ—the fraction of volumetric soil occupied by water. The soil thermal conductivity coefficient used in the model simulation for clay is 2.138, while the thermal conductivity coefficient for sand is 0.472 (see Table 4.1). The ground heat flux is therefore higher over clay soils than sandy soils, and energy is transferred to the atmospheric boundary layer at higher rates over clay soils as compared with sand. Sandy soil has many more pores and tends to be filled with air (with significantly less heat capacity as the soil dries) as compared to clay. This difference in the soil heat capacity and thermal conductivity coefficient largely

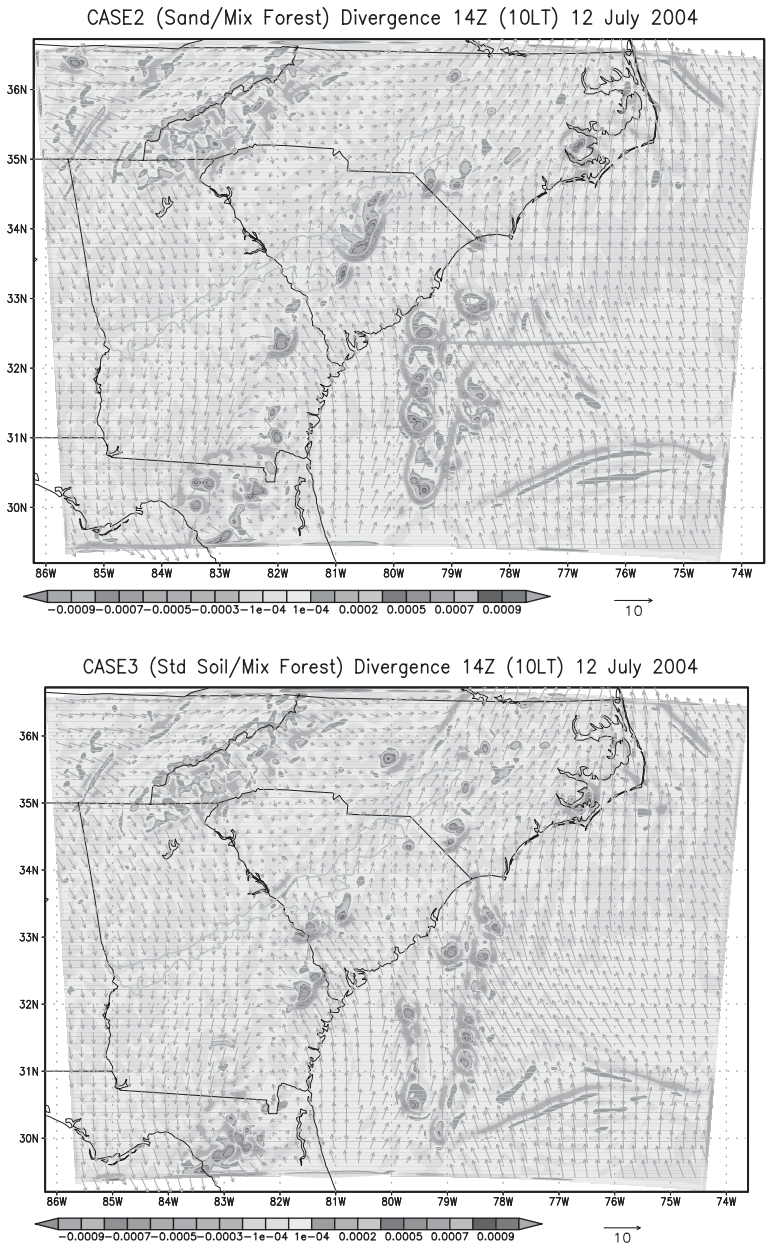

Figure 19
Surface winds and divergence for CASE2 (top) and CASE3 (bottom) simulations at 14Z (10 LT) on July 12, 2004.

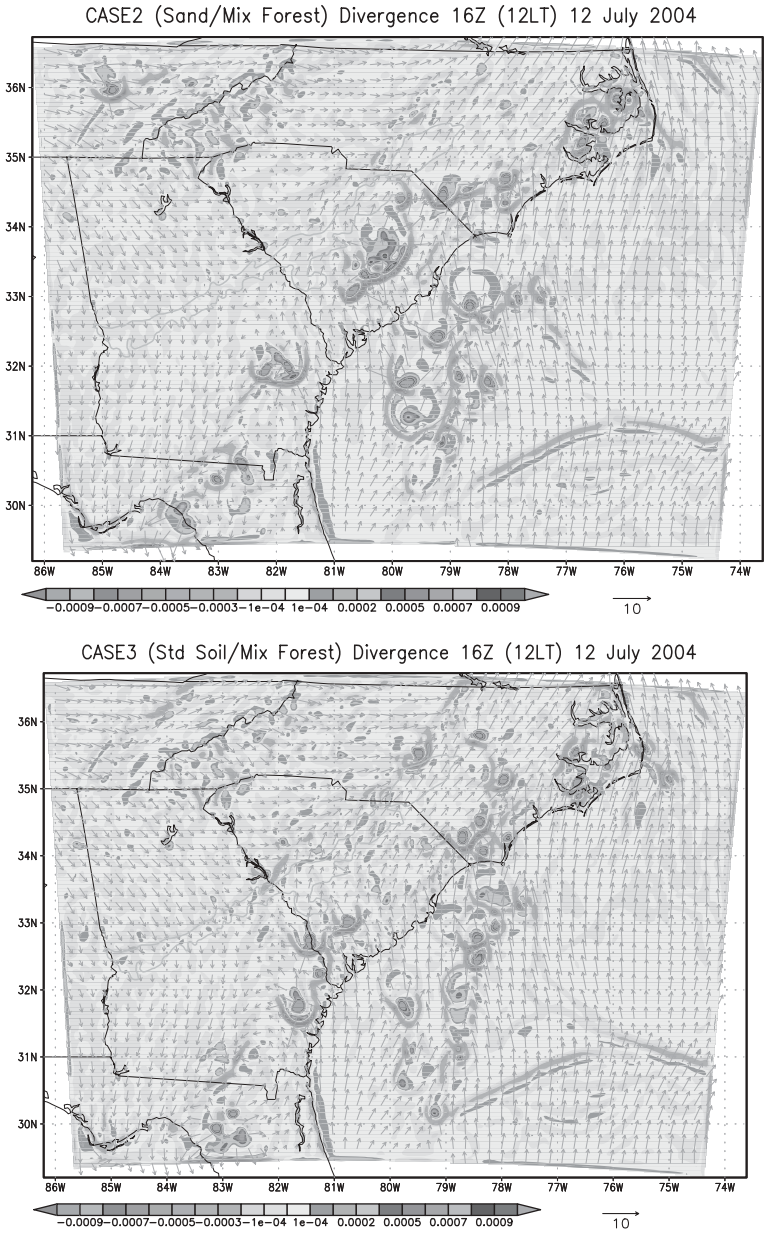

Figure 20
Surface winds and divergence for CASE2 (top) and CASE3 (bottom) simulations at 16Z (12 LT) on July 12, 2004.

accounts for the differences in surface heat fluxes in the model sensitivity simulations. In particular, the sensible heat flux gradients drive the vertical circulation in this region of contrasting soils by increasing local instability over clay soils similar to the role that land surface heating plays in the sea-breeze circulation. Over clay, the ground flux and change in storage is increased, which directly leads to higher ground temperatures and sensible heat fluxes. Schematically, the surface energy balance is represented below for sand (black) and clay (grey):

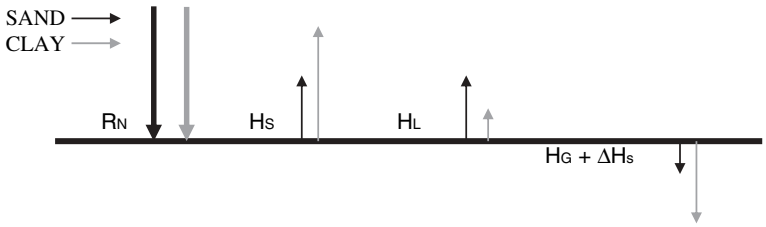

By adjusting the soil and vegetation patterns in three sensitivity simulations with the control simulation, several key conclusions can be drawn. Contrasting soils appear to play a larger role than contrasting vegetation in the partitioning of surface energy fluxes. There is evidence in the surface convergence patterns that the presence of the clay to sand transition zone over the Carolinas Sandhills may enhance surface convergence. However, it is important to note that the control simulation does not accurately handle observed precipitation locations and timing, although the areal averaged precipitation values compare well. Still, there is ample evidence to show the existence of surface heating variations due to the presence of contrasting soils, resulting in an increase in surface convergence associated with the transition zone from the sandy soils along the Carolina Sandhills to the clay soils in the Piedmont.

4. Conclusions

The Carolina Sandhills of NC, SC, and GA represent the transition between a primarily clay soil to the north and west and mostly sandy soils to the east and south. This transition has been suggested by others to be a region of enhanced precipitation during summer when synoptic forcing is weak. Previous modeling and climatology research have suggested that the variation in soil and vegetation patterns over this area may serve as a ''trigger'' for local convection.

Numerical weather simulations are analyzed to identify the sensitivity of the model atmosphere to variations in soil and vegetation patterns over the Carolina Sandhills. By comparing simulations with and without soil and vegetation contrasts with a control simulation of July 11–12, 2004, the atmospheric response to soil and

vegetation variations are isolated. Simulations reveal that the presence of the Sandhills and the transition from clay to sand in this region could support the dynamics needed for locally enhanced precipitation over this region. Local variations in soils are associated with heat flux gradients, which in turn affect local temperature and pressure gradients in a manner similar to a sea breeze circulation. The variation in pressure over the Sandhills leads to momentum and mass convergence that is observed in model wind and convergence fields. Simulations with contrasting soils showed surface heat flux gradients and increased surface convergence while simulations with uniform soils lacked these features.

References

Anthes, R. (1984), *Enhancement of convective precipitation by mesoscale variations in vegetative covering in semiarid regions,* J.Climate Appl. Meteor. *23*, 541–554.

Arya, S.P., *Introduction to Micrometeorology*, Second Edition (Academic Press, San Diego 2001), 415 pages.

Chen, F. and Dudhia, J. (2001), *Coupling an advanced land-surface/hydrology model with the Penn State/NCAR MM5 modelling system. Part I: Model Implementation and sensitivity,* Mon. Wea. Rev. *129*, 569–585.

Deardorff, J.W. (1978), *Efficient prediction of ground surface temperature and moisture with inclusion of a layer of vegetation*, J. Geophys. Res. *20*, 1889–1903.

Grell, G., Dudhia, J., and Stauffer, D. (1995), *A description of the the fifth-generation Penn State / NCAR mesoscale model (MM5)*, NCAR Technical Note NCAR/TN-398 + STR, 122 pp.

Hong, S.Y. and Pan, H.L. (1996), *Nonlocal boundary layer vertical diffusion in a medium-range forecast model*, Mon. Wea. Rev. *124*, 2322–2339.

Hong, X., Leach, M.J., and Raman, S. (1995), *Role of vegetation in generation of mesoscale circulation*, Atmos. Environ. *29*, 2163–2176.

Kain, J. S. and Fritsch, J. M., *Convective parameterization for mesoscale models: The Kain-Fritsch scheme. The representation of cumulus convection in numerical models* (eds. K. A. Emanuel and D. J. Raymond) (Am. Meteor. Soc. 1993), 246 pp.

Koch, S.E. and Ray, K. A. (1997), *Mesoanalysis of summertime convective zones in central and eastern North Carolina*, Wea. Forecasting *12*, 56–77.

Lin, Y. and Mitchell, K.E. (2005), *The NCEP Stage II/IV hourly precipitation analyses: Development and applications*. 19 Conf. *Hydrology*, San Diego, CA, Am. Meteor. Soc. 1.2.

Mahfouf, J.-F., Richard, E., and Mascart, P. (1987), *The influence of soil and vegetation on the development of mesoscale circulations*, J. Climate Appl. Meteor. *26*, 1483–1495.

Mlawer, E. J., Taubman, S. J., Brown, P.D., Iacono M. J. (1997), *Radiative transfer for inhomogeneous atmospheres: RRTM, a validated correlated-k model for the longwave*, J. Geophys. Res. *102*, 16663–16682.

Ookouchi, Y., Segal, M., Kessler, R.C., and Pielke, R.A. (1984), *Evaluation of soil moisture effects on the generation and modification of mesoscale circulations*, Mon. Wea. Rev. *112*, 2281–2292.

Raman, S., Sims, A., Ellis, R., and Boyles, R. (2005), *Numerical simulation of mesoscale circulations in a region of contrasting soil types*, Pure Appl. Geophys. *162*, 1689–1714.

Reisner, J., Rasmussen, R. J., and Bruintjes, R. T. (1998), *Explicit forecasting of supercooled liquid water in winter storms using the MM5 mesoscale model*, Quart. J. Roy. Meteor. Soc. *124B*, 1071–1107.

Segal, M., Avissar, R., McCumber, M.C., and Pielke, R.A. (1988), *Evaluation of vegetation effects on the generation and modification of mesoscale circulations*, J. Atmos. Sci. *45*, 2268–2293.

Schultz, P. (1995), *An explicit cloud physics parameterization for operational numerical weather prediction*, Mon. Wea. Rev. *123*, 3331–3343.

SIMS, A. (2001), *Effect of mesoscale processes on boundary layer structure and precipitation patterns : A diagnostic evaluation and validation of MM5 with North Carolina ECONet observations*. Masters Thesis, Department of Marine, Earth, and Atmospheric Sciences, North Carolina State University.

(Received April 1, 2006, accepted November 14, 2006)
Published Online First: July 19, 2007